Ionic Liquid Crystal Precursors for Inorganic Particles: Phase Diagram and Thermal Properties of a CuCl Nanoplatelet Precursor

Andreas Taubert,* Pascal Steiner, and Alexandre Mantion

Department of Chemistry, University of Basel, Klingelbergstrasse 80, CH-4056 Basel, Switzerland

Received: March 11, 2005; In Final Form: May 10, 2005

We have recently reported (*Angew. Chem. Int. Ed.* **2004**, *43* (40), 5380) the formation of CuCl nanoplatelets from an ionic liquid crystal precursor (ILCP) consisting of a 50/50 (wt/wt) mixture of bis(dodecylpyridinium) tetrachlorocuprate **1** and 6-*O*-palmitoyl ascorbic acid **2**. Here we present the full ILCP phase diagram and the thermal behavior from a mixing ratio of 1/0 (i.e., pure **1**) to 0/1 (i.e., pure **2**). The ILCP exhibits a crystalline−smectic−isotropic phase transition at all mixing ratios, and the liquid crystal region is up to 90 °C wide. DSC shows a broad exothermic peak between ca. 70 and 170 °C, which is associated with the thermally induced CuCl formation. The reaction enthalpies reach −150 kJ/mol at around 50/50 (wt/wt) mixtures of the two components, and the activation energy for CuCl formation is ca. 190 kJ/mol. Thermogravimetric analysis shows that the samples degrade above ca. 200 °C.

Introduction

Ionic liquids (ILs) have been widely promoted as green and efficient solvents for many reactions in organic chemistry, for electrochemical applications, or for industrial extraction problems.[1] Ionic liquid crystals (ILCs), i.e., ionic liquids with a long-range order, have also been studied in some detail by Neve et al.,[2−6] Lee et al.,[7] Seddon et al.,[8−12] and a few other groups.[13−16] For a recent review about the structural organization in ionic liquids see also ref 17.

More recently, ILs have also been investigated by the (inorganic) materials community because ILs can easily be tuned to interact with various surfaces and chemical environments. Inorganic materials chemistry has mainly focused on the fabrication and stabilization of ordered metal oxides[18−22] or metal, metal alloy, metal oxide, and metal sulfide nanoparticles.[23−33] These developments have recently also been reviewed.[34]

Combining ILCs and inorganic materials chemistry, we have recently reported the formation of an ILC from a 50/50 (wt/wt) mixture of bis(dodecylpyridinium) tetrachlorocuprate **1** and 6-*O*-palmitoyl ascorbic acid **2**, Scheme 1.[35] We have suggested from the analysis of the optical micrographs and from interpolation of the self-assembly behavior of the individual components **1** and **2** that the mixture forms a layered LC. Furthermore, this so-called ionic liquid crystal precursor (ILCP) templates the formation of CuCl nanoplatelets at elevated temperatures, which further supports the claim of a layered ILCP.

Here we present a detailed study on the structure and reactivity of these ILCPs. Specifically, we use an improved method to fabricate the mixtures of **1** and **2** and report on the full phase diagram and the thermal behavior of the ILCPs.

Experimental Section

Compound **1** was obtained as described previously,[35] but we have increased the reaction time from 10 to 60 min. 6-*O*-Palmitoyl ascorbic acid **2** was obtained from Fluka and used without further purification. Instead of mechanically mixing the two components to obtain the ILCP, **1** and **2** were dissolved in THF, the THF was removed by rotary evaporation, and the resulting dark brownish to light yellow materials were dried under vacuum overnight. The samples obtained with this procedure are more homogeneous than those employed in our previous study. Solutions of **1** and **2** in THF are stable without any visible precipitation for up to 5 months. Thereafter, a green precipitate forms. In the remainder of the text, samples are labeled Cu###, where ### is the weight fraction of **1** in the respective mixture. Cu000 thus designates pure **2**, Cu020 is a 20/80 (wt/wt) mixture of **1** and **2**, etc.

SCHEME 1: Bis(dodecyl pyridinium) Tetrachlorocuprate 1 and 6-*O*-Palmitoyl ascorbic Acid 2

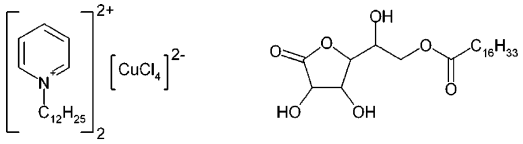

1 **2**

Optical polarization microscopy (OPM) experiments were made on a Leica DM-RP microscope with a hotstage. DSC experiments were made on a Perkin-Elmer DSC 6 calibrated with indium. Typically, measurements were done from −5 to 200 °C with a heating rate of 10 °C/min. Samples were held at −5 °C for 120 min before the first and 15 min before the second heating cycle. Reaction enthalpies were calculated by using an apparent molecular weight of the mixture of **1** and **2** computed from the molecular weights (702.2 and 430.6 g/mol, respectively) and the weight fractions of the two components in each mixture. Activation energies for CuCl formation were determined via the Kissinger peak method[36] with heating rates of 5, 10, 20, and 30 °C/min. Measurements were done with Cu050; repeat measurements showed that the peak temperature, T_p, is reproducible to ±2 °C and in most cases to ±1 °C. Thermogravimetric analysis (TGA) was done with a Mettler Toledo TGA/SDTA 851e from 25 to 300 °C with a heating rate of 10

* Corresponding author. E-mail: andreas.taubert@unibas.ch. Tel: ++41 (0)61 267 38 32. Fax: ++41 (0)61 267 38 55.

10.1021/jp051262w CCC: $30.25
Published on Web 07/27/2005

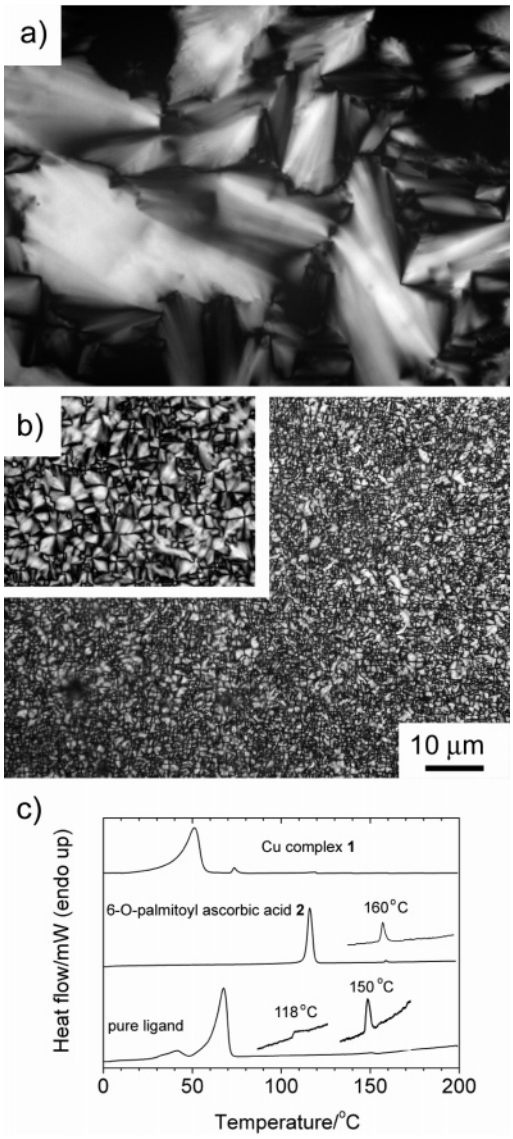

Figure 1. (a) Optical micrograph (crossed polarizers) of the ligand dodecylpyridinium chloride at 110 °C. (b) Optical micrograph (crossed polarizers) of pure **2** at 134 °C; the scale bar applies to (a) and (b). Inset: magnified view of the texture of **2**. (c) DSC first heating trace of **1**, **2**, and dodecylpyridinium chloride. Insets show the endothermic peaks associated with the further transitions mentioned in the text.

°C/min in N_2. Estimations of the molecular dimensions were done with ChemOffice Chem3D.

X-ray scattering experiments were done at the powder diffraction station of the Swiss Light Source's (Paul Scherrer Institute, Villigen) materials science beamline X04SA equipped with the new MYTHEN microstrip detector.[37] For scattering experiments, samples were mounted on 1 mm mark tubes (Hilgendorf) and measured at room temperature while rotating the sample. Beam energy was 17.5 keV, and the X-ray wavelength λ was 0.708 Å. Typical measurement times were 10 or 20 s. Further low-angle X-ray experiments were done on a Siemens D5000 using Cu Kα radiation (λ = 1.5408 Å).

Results and Discussion

Pure Components. Figure 1 shows OPM images and DSC traces of **1**, **2**, and the ligand dodecyl pyridinium chloride. **1** melts at 50−53 °C and has a liquid crystal−isotropic (LC−iso) transition at 74−76 °C. Despite the different sample preparation procedure, the melting point and the LC−iso transition temperature are consistent with the literature,[3−5] but deviate somewhat from our earlier melting point of 66−70 °C.[35] We explain this with the improved sample preparation, where we have allowed for a longer reaction time.

2 melts at 113−116 °C, and the liquid crystal (LC) observed above the melting temperature has a clear point at 160 °C in the OPM. Correspondingly, DSC shows an endothermic peak (ΔH = 0.8 kJ/mol) at 160 °C. This is to the best knowledge of the authors the first report on a thermotropic LC from an ascorbic acid derivative, but lyotropic phases have been described.[38]

The pure ligand dodecylpyridinium chloride melts at 60−65 °C. DSC of the ligand also shows endothermic peaks at 118 °C (ΔH = 0.5 kJ/mol) and 150 °C (ΔH = 1.3 kJ/mol), which indicates a crystalline −LC1−LC2− isotropic transition, where the transition temperatures are 65, 118, and 150 °C, respectively. OPM images support this interpretation, as they show an LC texture between 65 and 117−120 °C. We currently assign the texture to a smectic liquid crystal. Above 120 °C, the mixture is isotropic in OPM; we may thus infer that LC2, which is detected in the DSC, has another, nonbirefringent, symmetry.

ILCPs. We will now focus on the mixtures of **1** and **2**, i.e., the ILCPs. They are light yellow at low weight fractions of the Cu complex **1** and become increasingly dark yellow to brown on increasing concentration of **1**. Cu010, Cu020, Cu030, Cu080, and Cu090 have a waxlike appearance and easily break into smaller pieces. The other mixtures are honeylike and flow under the pressure of a spatulum.

Phase Diagram. Figures 2a−2d are representative OPM images of various ILCPs. At 20 °C and below, only Cu 040, Cu050, Cu060, and Cu070 exhibit an LC texture and the other samples appear crystalline in the OPM. Above ca. 30 °C all ILCPs exhibit a single LC texture up to the clear point. This is similar to pure **1**, where only one LC is observed.[3,4] We currently assign our textures to smectic LCs, even though often they are not very characteristic and even though pure **1** is columnar.[3] Our assignment is however supported by X-ray scattering (see Figure 4). Furthermore, bis(hexadecylpyridinium) tetrachlorocuprate, i.e., the C_{16} analogue of **1** with the same alkyl tail length as **2**, exhibits a SmA phase.[3]

DSC of the ILCPs reveals a broad endothermic phase transition from ca. 5 up to 40 °C; see Figure 2e. We assign this transition to the crystalline−Sm transition observed in the OPM. DSC thus confirms the presence of a broad crystalline−Sm phase transition just around room temperature.

Figure 3 is the ILCP phase diagram obtained from OPM and DSC. All ILCPs exhibit a crystalline−Sm−isotropic transition, and the LC region is largest (up to 90 °C) at weight fractions of **1** between 0.3 and 0.7. The error bars correspond to the breadth of the transition observed in the DSC; they show that some of the transitions are broad, which makes them difficult to observe in the OPM. This applies in particular to the crystal−LC transition, whereas the LC−iso transition is clearly visible in the OPM.

Structure of the ILCP. Figure 4 shows the X-ray patterns of Cu050 and Cu090. Cu090 is representative of samples at either end of the phase diagram; Cu050 for ILCPs at the center of the phase diagram. The pattern of Cu050 exhibits two reflections at 2.67 and 5.29 degrees 2θ, which we assign to the 100 and 200 reflection of a layered LC with a spacing of 33.1 Å.

However, even with a fully extended C_{16} chain, **2** (the longest molecule in the system) is only 28.7 Å long, which is 4.4 Å shorter than the long period of the LC of 33.1 Å. This

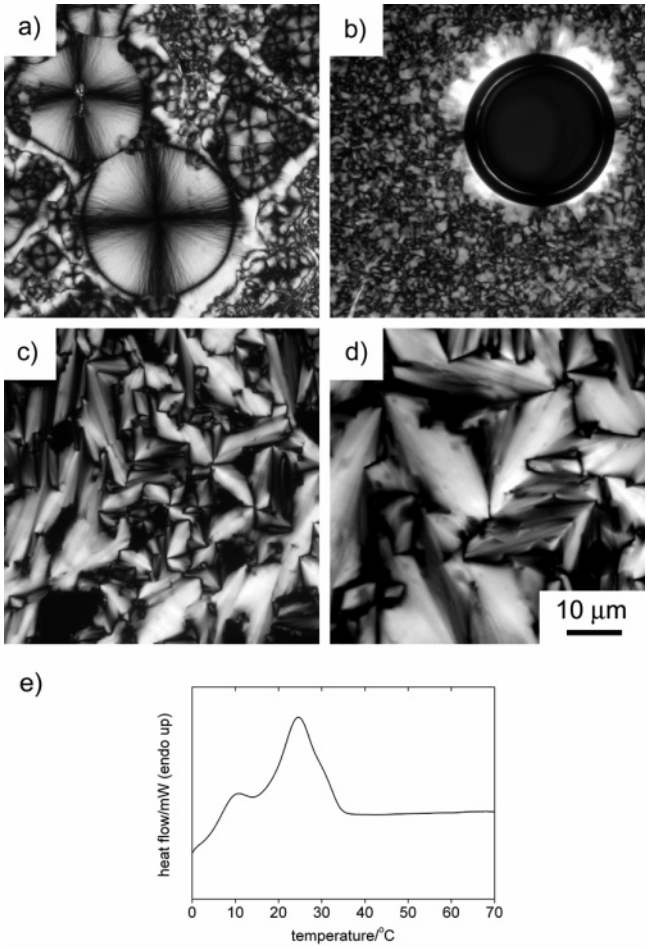

Figure 2. Representative optical micrographs (crossed polarizers) of (a) pure **2** at room temperature after slow cooling from 150 °C, (b) Cu050 at 85 °C on first heating, (c) Cu060 at 69 °C on rapid cooling from the isotropic melt, and (d) Cu070 on rapid cooling from the isotropic melt at 60 °C. The scale bar applies to all images. (e) DSC peak of the melting transition of Cu050 showing that the transition is broad.

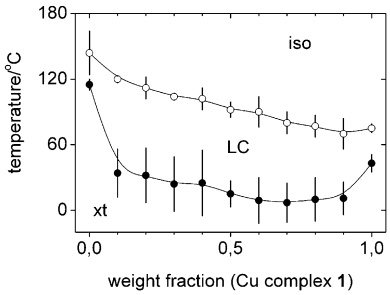

Figure 3. Phase diagram of ILCPs of **1** and **2** obtained from OPM and DSC. Xt: crystalline region, LC: liquid crystalline region, iso: isotropic region (dark in the OPM). The error bars give the width of the observed transition, i.e., the range between the onset and the upper end of the corresponding DSC peak (see Figure 2e for a typical melting peak width).

discrepancy can be accounted for in different ways: (i) if the $CuCl_4^{2-}$ counterion is loosely bound in the LC, the layer spacing could be larger than the calculated molecular length of the longest component. However, 4.4 Å is a large difference between observed and calculated spacings. It is thus more likely that (ii) **1** and **2** form a mixed tilted bilayer with a layer spacing of 33.1 Å. This assumption is supported by Chem3D measurements showing that an untilted bilayer of **2** is 37−38 Å thick, which is ca. 5 Å thicker than the X-ray thickness (see Supporting Information). The most straightforward way to obtain a layered structure with a spacing of 33.1 Å would thus be tilting.

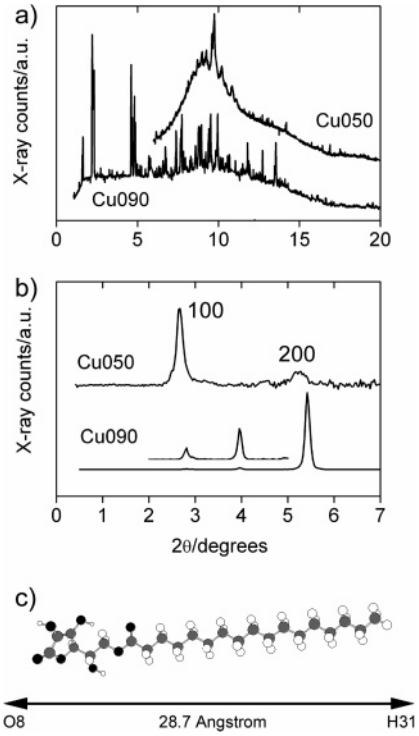

Figure 4. (a) Representative synchrotron ($\lambda = 0.708$ Å) X-ray patterns of Cu090 and Cu050 at room temperature. The lower end of the Cu050 pattern has been cut for clarity. (b) Low-angle pattern of Cu050 and Cu090. These patterns were acquired with Cu Kα radiation ($\lambda = 1.5408$ Å), and the signals are thus shifted with respect to the reflections observed in the above pattern. (c) Calculated structure of **2** with a fully extended C_{16} chain. White: hydrogen, gray: carbon, black: oxygen.

Besides the low-angle reflection, the pattern of Cu050 shows a broad hump at ca. 10 degrees 2θ, which we assign to the liquidlike alkyl tails of **1** and **2**. The pattern also shows a few reflections that we cannot assign to an LC phase; we assign them to the fact that these samples are still partly crystalline at room temperature. This is consistent with OPM and DSC, which also show that the crystalline−LC phase transition occurs over a rather broad temperature range between 5 and ca. 40 °C; see Figure 2e.

Unlike ILCPs from the center of the phase diagram, ILCPs with either low or high weight fractions of **1** (Cu010, Cu020, Cu030, Cu080, Cu090) exhibit X-ray patterns with many reflections but with a much less intense hump around 10 degrees. This clearly indicates that these materials are predominantly crystalline. As we have not been able to obtain either single crystals or a calculated structure of the mixed systems, the detailed structure of the crystalline phase is still undetermined.

Overall however, X-ray supports OPM data presented above. X-ray shows that the samples from the center of the phase diagram are predominantly, but not completely, liquid crystalline at room temperature, but samples from either end of the phase diagram are crystalline. X-ray also confirms the assignment of a layered LC phase.

The ILCPs are difficult to investigate because they not only exhibit mesomorphism but are also reactive matrixes for CuCl formation.[35] Unlike conventional LCs, we cannot anneal the ILCPs below the LC−isotropic transition temperature to obtain characteristic textures, because heating to over ca. 50 °C induces CuCl formation. In fact, continued heating destroys the me-

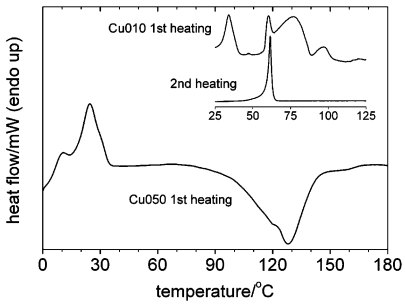

Figure 5. Representative first heating curve of Cu050. The DSC traces exhibit a broad peak from ca. 5 up to 40 °C and a broad exothermic peak between ca. 70 and 170 °C. The inset shows the additional endothermic peaks observed in Cu010 and Cu020 on first heating and a typical second heating curve; both are from Cu010.

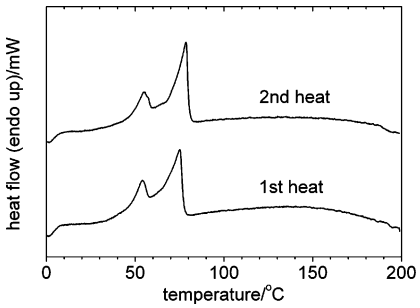

Figure 6. DSC traces of a 1:2 (wt/wt) mixture of **2** and dodecylpyridinium chloride.

sophase and crystals become visible in the optical microscope (data not shown). Figures 3 and 4 thus refer to an *unreacted* mixture.

Thermal Properties. Figure 5 shows a DSC trace of Cu050. Like all other samples, Cu050 exhibits a broad endotherm from 5 to ca. 40 °C (the melting peak) and a broad exotherm between ca. 70 and 175 °C (due to the formation of CuCl particles) on first heating. The peak temperature, T_p, of the exothermic peak lies between 120 and 130 °C. Only in Cu090 is the T_p at 155 °C.

In addition to the endothermic peak at around room temperature, Cu010 and Cu020 show three endothermic peaks between 55 and 110 °C on first heating; see the inset in Figure 5. The first peak is sharp and centered around 60 °C, the second peak is broad and centered around 75 °C, and the last peak is at ca. 100 °C and much less intense. On second heating all samples exhibit a sharp endothermic peak between 55 and 65 °C. Finally, Cu050 and Cu060 exhibit a weak exothermic peak at ca. 100−110 °C also on second heating.

We have performed DSC experiments with mixtures of **2** and the pure ligand, i.e., in the *absence* of a reactive Cu(II) center, to elucidate the origin of the various additional peaks in the thermograms of Cu010 and Cu020. Figure 6 shows that mixtures of the pure ligand dodecyl pyridinium chloride and **2** often exhibit a double peak on both first and second heating. By comparison with the data from Figure 1, we assign the smaller peak at 55 °C to the melting of some dodecyl pyridinium chloride. We do not observe a melting peak due to pure **2** (113−116 °C), and we assign the more intense peak at ca. 75 °C to the melting transition of the mixture of **2** and the ligand. The samples are thus quite homogeneous because only a minor fraction of one compound (the ligand) shows an individual melting transition. More importantly, the mixture melts at a temperature similar to where the sharp peak on second heating is observed in the Cu-containing ILCPs; see the inset in Figure 5.

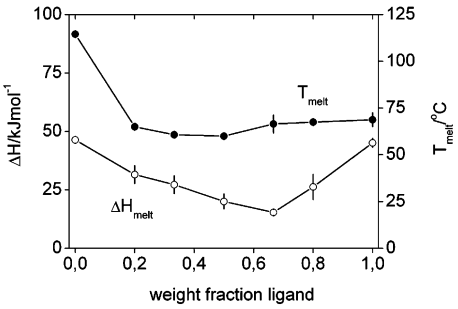

Figure 7. Mean melting temperatures (T_{melt}) and mean ΔH_{melt} values of various mixtures of pure ligand and **2**. Values and errors were determined from the most intense peak (see Figure 6) and by averaging data from three measurements.

Figure 7 shows that the melting temperature of the mixtures of **2** and dodecylpyridinium chloride (i.e., the peak position of the more intense peak in Figure 6) only weakly depends on the mixing ratio. For example, the addition of 20 wt % of dodecylpyridinium chloride (the pure ligand) to **2** reduces T_{melt} to 65 °C. Higher weight fractions of ligand do not dramatically alter this temperature, as all melting temperatures of the mixtures are between 60 and 75 °C. This further supports the interpretation that the peak observed in the DSC of the ILCPs on second heating is due to a mixture of ligand and (oxidized) **2**.

By combination of the data above, we now propose an explanation for the additional peaks observed in the DSC curves of Cu010 and 020 and for the sharp peak observed in all samples on second heating. On first heating, the sharp peak observed at 55−65 °C in the thermograms of Cu010 and Cu020 can be assigned to the melting of the pure ligand dodecylpyridinium chloride by comparison to Figure 1. The broad peak around 75 °C is most likely due to a mixture of **2** and the pure ligand, i.e., without copper; see Figures 6 and 7. We can rule out the possibility that the latter peak arises from the LC−iso transition in pure **1** (73−75 °C) because ΔH is far too large for an LC−iso transition. The peak at ca. 100 °C could be from some free crystals of **2**. If this, currently rather speculative, assignment is correct, the crystals are probably small because the melting temperature is ca. 10 °C lower than in bulk **2**.

Finally, the sharp peak observed on second heating in all samples is caused by a mixture of free ligand (released from **1** on CuCl formation) and (oxidized) **2**. This mixture melts at 55−65 °C, i.e., the location of the sharp peak in the traces of Cu010 and Cu020 and in all DSC second heating traces.

The presence of free ligand in the ILCPs suggests that during sample preparation from THF some ligands are released from **1**. This could imply a disproportionation reaction leading to dodecylpyridinium chloride and a dodecylpyridinium−$CuCl_3^-$ complex. Possibly, the ascorbic acid headgroups of **2** interact with the disproportionation complex and lead to a (dodecylpyridinium−$CuCl_3^-$) (**2**) adduct. If this is indeed the case, we may postulate that such centers could act as the nucleation sites for CuCl precipitation, as here the reducing agent is already in close contact with a Cu(II) ion. This hypothesis is currently being verified with EPR, IR, UV, and solid-state NMR.

Figure 8 shows ΔH values for the melting (ΔH_{endo}) and exothermic (ΔH_{exo}) transitions as a function of ILCP composition. ΔH_{endo} decreases from 45 to 4 kJ/mol with increasing weight fractions of **1** on first heating. On second heating, the ΔH_{endo} values (in this case from the sharp peaks at 55−65 °C) show the same trend and range from 88 to 15 kJ/mol. The values are roughly comparable to bis(hexadecylpyridinium) tetrachlorocuprate (ΔH_{melt} = 51.7 kJ/mol) and to **1** (ΔH_{melt} = 29.3 kJ/

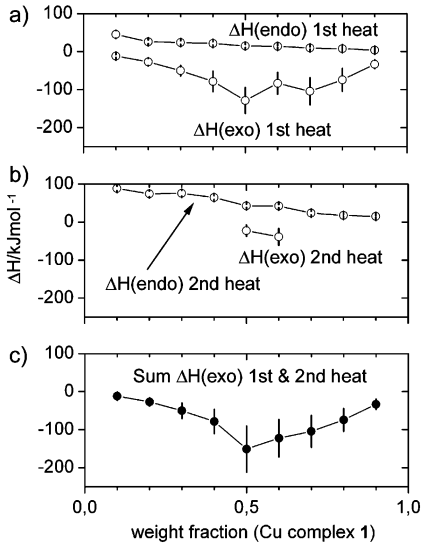

Figure 8. (a) ΔH values for ILCPs on first heating. (b) ΔH values for ILCPs on second heating. (c) Sum of ΔH_{exo} values for ILCPs on first and second heating.

mol),[3] but they span a much larger window. For comparison, Figure 7 also shows that the melting enthalpies of the mixtures of pure ligand and **2** decrease up to a ligand weight fraction of 0.66, after which they increase again to approximately 45 kJ/mol for the free ligand, i.e., they are comparable to the ILCPs.

Unlike the approximately linear behavior of ΔH_{endo}, ΔH_{exo} values have a minimum at Cu050 and Cu070 on first heating. ΔH_{exo} of Cu060 is reproducibly higher than either one of the latter values on first heating. On second heating, only Cu050 and Cu060 exhibit a measurable and reproducible exothermic peak. The *sum* of the measured exothermic signals from the first and second heating has only one minimum of −151 kJ/mol at Cu050. An ILCP with a molar ratio of 1:1 contains 62 wt % of **1**, and one would thus expect the largest reaction enthalpy in Cu060. However, as the error bars are relatively large around Cu050, the difference is likely within the experimental error.

From DSC it is also possible to estimate the activation energy, E_a, of CuCl formation. Because the exothermic peaks are broad and the onset of the exothermic peak is poorly defined, we have used the quite simple Kissinger peak method,[36] even though there are more advanced approaches for the determination of E_a available.[39,40] In the Kissinger method, the peak temperatures, T_p, of the exothermic peak are determined at different heating rates, β. A plot of $1/T_p$ vs $\ln(T_p^2/\beta)$ is linear, and the slope of the linear regression gives E_a/R ($R = 8.314$ J/K·mol), from which the activation energy, E_a, is obtained.

Figure 9 shows the Kissinger plot of a fresh Cu050 and a sample that was aged for six weeks at room conditions. The activation energies are 190.8 kJ/mol for the fresh and 192.4 kJ/mol for the aged sample; they are comparable, which indicates that at ambient conditions the formation of CuCl is strongly inhibited and does not proceed even after extended storage time. Other solid−solid transformations have activation energies between 30 and over 300 kJ/mol. For example the activation energy for the precipitation in copper−chromium alloys is ca. 120 kJ/mol in undeformed alloys[41] and a quasicrystalline−crystalline phase transition in Al_6CuMg_4 is ca. 260 kJ/mol.[42] While the activation energy obtained here is thus not exceedingly high, it certainly points to a cooperative effect,[40] i.e., the nucleation and growth of CuCl crystals within the ILCP.

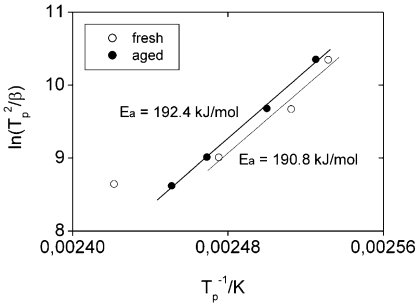

Figure 9. Kissinger plot obtained from averaging three measurements per heating rate of a freshly prepared Cu050 and a Cu050 aged for 6 weeks at room temperature and ambient pressure and humidity. The peak temperatures are reproducible to within ±2 °C, and the error bars are thus smaller than the dot size. In the fresh sample, heating rates of 30 °C/min and above could not be evaluated, as there, T_p shows a nonlinear behavior (see for example the open circle on the far left). In the aged sample, heating rates of 40 °C/min and more were not evaluated for the same reason.

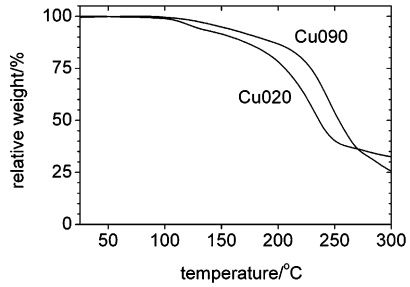

Figure 10. Representative TGA curves of Cu020 and Cu090.

Finally, we have evaluated the thermal stability of our samples using thermogravimetric analysis (TGA), Figure 10. All samples lose between 6 and 12% of their original weight (presumably water) between 110 and 125 °C, and all samples lose 45−60% of the original weight above ca. 180 °C. The latter process is important because we have studied the samples up to 200 °C in the DSC.

However, the sharp peak observed in the DSC on second heating (see inset in Figure 5) is not due to a decomposition product, as DSC experiments with mixtures of dodecylpyridinium chloride and **2** that were held at 150 °C rule out this possibility. The temperature of 150 °C is below the presumed decomposition temperature of 180 °C, and these mixtures do not contain a reactive Cu(II) ion. Nevertheless, these samples exhibit the same peak on second heating as the samples heated to 200 °C.

Conclusion

The current paper shows not only that Cu050, the original ILCP used for CuCl platelet formation,[35] exhibits mesomorphism but that all ILCPs composed of **1** and **2** show the same general crystalline−smectic LC−isotropic phase behavior. The system is fairly complicated because thermal reduction of **1** by **2** leads to CuCl, oxidized forms of **2**, HCl, and Cl^-. As the reaction proceeds by heating the mixture, DSC measurements are not equilibrium measurements, and the contributions of the reaction products vary as the reaction proceeds. These issues are currently being addressed by time-resolved in-situ high-temperature X-ray, solid-state NMR, IR, and UV measurements as well as with ex situ mass spectrometry (MS) and GC-MS experiments.

However, our data show that the system is stable at ambient conditions and that the thermally induced formation of CuCl

already occurs in a controlled manner at temperatures well below 100 °C. As the ILCPs can be dissolved in THF, one may thus envision applications where the ILCP is cast onto a surface and reacted at 50−80 °C, yielding a (macro)porous CuCl network, which can be removed from the surface and used, for example, as a heterogeneous catalyst. We are currently exploring these possibilities along with ILCPs with other symmetries that could lead to other morphologies of the final inorganic.

Acknowledgment. The authors thank Prof. W. Meier (U. of Basel) and Dr. A. R. McGhie (U. of Pennsylvania) for useful discussions, Prof. W. B. Stern (U. of Basel) for access to the X-ray setup at the Earth Sciences Department, Prof. K. Fromm (U. of Basel) for access to her TGA, and Dr. F. Gozzo, Dr. B. Patterson, and Dr. B. Schmitt (Swiss Light Source, Villigen) for help with the synchrotron experiments. We also thank the Swiss National Science Foundation for financial support, and A.T. acknowledges the Holcim Stiftung Wissen for a Habilitation Fellowship.

Supporting Information Available: A graph of a calculated bilayer of **2** and a mixed bilayer. This material is available free of charge via the Internet at http://pubs.acs.org.

References and Notes

(1) *Ionic Liquids in Synthesis*; Wiley-VCH: Weinheim, 2002.
(2) Neve, F.; Crispini, A.; Armentano, S. *Chem. Mater.* **1998**, *10*, 1904.
(3) Neve, F.; Francescangeli, O.; Crispini, A.; Charmant, J. *Chem. Mater.* **2001**, *13*, 2032.
(4) Neve, F.; Francescangeli, O.; Crispini, A. *Inorg. Chim. Acta* **2002**, *338*, 51.
(5) Neve, F.; Imperor-Clerc, M. *Liq. Cryst.* **2004**, *31*, 907.
(6) Neve, F.; Francescangeli, O. *J. Cryst. Growth* **2005**, *5*, 163.
(7) Lee, C. K.; Peng, H. H.; Lin, I. J. B. *Chem. Mater.* **2004**, *16*, 530.
(8) Bowlas, C. J.; Bruce, D. W.; Seddon, K. R. *Chem. Commun.* **1996**, 1625.
(9) Gordon, C. M.; Holbrey, J. D.; Kennedy, A. R.; Seddon, K. R. *J. Mater. Chem.* **1998**, *8*, 2627.
(10) Holbrey, J. D.; Seddon, K. R. *J. Chem. Soc., Dalton Trans.* **1999**, 2133.
(11) Carmichael, A. J.; Hardacre, C.; Holbrey, J. D.; Nieuwenhuyzen, M.; Seddon, K. R. *Mol. Phys.* **2001**, *99*, 795.
(12) Hardacre, C.; Holbrey, J. D.; McCormac, P. B.; McMath, S. E. J.; Nieuwenhuyzen, M.; Seddon, K. R. *J. Mater. Chem.* **2001**, *11*, 346.
(13) Bowers, J.; Butts, C. P.; Martin, P. J.; Vergara-Gutierrez, M. C.; Heenan, R. K. *Langmuir* **2004**, *20*, 2191.
(14) Yoshio, M.; Mukai, T.; Ohno, H.; Kato, T. *J. Am. Chem. Soc.* **2004**, *126*, 994.
(15) Firestone, M. A.; Dzielawa, J. A.; Zapol, P.; Curtiss, L. A.; Seifert, S.; Dietz, M. L. *Langmuir* **2002**, *18*, 7258.
(16) Yoshio, M.; Mukai, T.; Kanie, K.; Yoshizawa, M.; Ohno, H.; Kato, T. *Chem. Lett.* **2002**, 320.
(17) Dupont, J. *J. Braz. Chem. Soc.* **2004**, *15*, 341**.**
(18) Nakashima, T.; Kimizuka, N. *J. Am. Chem. Soc.* **2003**, *125*, 6386.
(19) Zhou, Y.; Antonietti, M. *Adv. Mater.* **2003**, *15*, 1452.
(20) Zhou, Y.; Antonietti, M. *Chem. Commun.* **2003**, 2564.
(21) Zhou, Y.; Antonietti, M. *J. Am. Chem. Soc.* **2003**, *125*, 14960.
(22) Dai, S.; Ju, Y. H.; Gao, H. J.; Lin, J. S.; Pennycook, S. J.; Barnes, C. E. *Chem. Commun.* **2000**, 243.
(23) Dupont, J.; Fonseca, G. S.; Umpierre, A. P.; Fichtner, P. F. P.; Teixeira, S. R. *J. Am. Chem. Soc.* **2002**, *124*, 4228.
(24) Desmukh, R. R.; Rajagopal, R.; Srinivasan, K. V. *Chem. Commun.* **2001**, 1544.
(25) Swatloski, R. P.; Spear, S. K.; Holbrey, J. D.; Rogers, R. D. *J. Am. Chem. Soc.* **2002**, *124*, 4974.
(26) Fonseca, G. S.; Umpierre, A. P.; Fichtner, P. F. P.; Teixeira, S. R.; Dupont, J. *Chem. Eur. J.* **2003**, *9*, 3263.
(27) Scheeren, C. W.; Machado, G.; Dupont, J.; Fichtner, P. F. P.; Ribeiro Texeira, S. *Inorg. Chem.* **2003**, *42*, 4738.
(28) Rossi, L. M.; Dupont, J.; Machado, G.; Fichtner, P. F. P.; Radtke, C.; Baumvol, I. J. R.; Teixeira, S. R. *J. Braz. Chem. Soc.* **2004**, *15*, 904.
(29) Trewyn, B. G.; Whitman, C. M.; Lin, V. S.-Y. *Nano Lett.* **2004**, *4*, 2139.
(30) Yoo, K.; Choi, H.; Dionysiou, D. D. *Chem. Commun.* **2004**, 2000.
(31) Cassol, C. C.; Umpierrre, A. P.; Machado, G.; Wolke, S. I.; Dupont, J. *J. Am. Chem. Soc.* **2005**, *127*, 3298.
(32) Jiang, Y.; Zhu, Y.-J. *J. Phys. Chem. B* **2005**, *109*, 4361.
(33) Wang, Y.; Yang, H. *J. Am. Chem. Soc.* **2005**, *127*, 5316.
(34) Antonietti, M.; Kuang, D.; Smarsly, B.; Zhou, Y. *Angew. Chem., Int. Ed.* **2004**, *43*, 4988.
(35) Taubert, A. *Angew. Chem., Int. Ed.* **2004**, *43*, 5380.
(36) Kissinger, H. E. *J. Res. Natl. Bur. Stand.* **1956**, *57*, 217.
(37) Schmitt, B.; Brönnimann, C.; Eikenberrya, E. F.; Gozzo, F.; Hörmann, C.; Horisberger, C.; Patterson, B. *Nucl. Instrum. Methods Phys. Res. A* **2003**, *501*, 267.
(38) Lo Nostro, P.; Ninham, B. W.; Fratoni, L.; Palma, S.; Hilario Manzo, R.; Allemandi, D.; Baglioni, P. *Langmuir* **2003**, *19*, 3222.
(39) Shanker Rao, T. L.; Lad, K. N.; Pratap, A. *J. Therm. Anal. Calorim.* **2004**, *78*, 769.
(40) Starink, M. J. *Thermochim. Acta* **2003**, *404*, 163.
(41) Szablewski, J.; Kuznicka, B. *Phys. Status Solidi A* **1988**, *108*, K5.
(42) Sanyal, M. K.; Sahni, V. C.; Dey, G. K.; Varshney, L. *Phys. Rev. B* **1987**, *36*, 2443.